Iron Particle Size Effects for Direct Production of Lower Olefins from Synthesis Gas

Hirsa M. Torres Galvis,[†] Johannes H. Bitter,[†] Thomas Davidian,[‡] Matthijs Ruitenbeek,[‡] A. Iulian Dugulan,[§] and Krijn P. de Jong*,[†]

[†]Inorganic Chemistry and Catalysis, Debye Institute for Nanomaterials Science, Utrecht University, Universiteitsweg 99, 3584 CG, Utrecht, The Netherlands

[‡]Dow Benelux B.V., P.O. Box 48, 4530 AA, Terneuzen, The Netherlands

[§]Fundamental Aspects of Materials and Energy Group, Delft University of Technology, Mekelweg 15, 2629 JB, Delft, The Netherlands

S *Supporting Information*

ABSTRACT: The Fischer−Tropsch synthesis of lower olefins (FTO) is an alternative process for the production of key chemical building blocks from non-petroleum-based sources such as natural gas, coal, or biomass. The influence of the iron carbide particle size of promoted and unpromoted carbon nanofiber supported catalysts on the conversion of synthesis gas has been investigated at 340−350 °C, $H_2/CO = 1$, and pressures of 1 and 20 bar. The surface-specific activity (apparent TOF) based on the initial activity of unpromoted catalysts at 1 bar increased 6−8-fold when the average iron carbide size decreased from 7 to 2 nm, while methane and lower olefins selectivity were not affected. The same decrease in particle size for catalysts promoted by Na plus S resulted at 20 bar in a 2-fold increase of the apparent TOF based on initial activity which was mainly caused by

a higher yield of methane for the smallest particles. Presumably, methane formation takes place at highly active low coordination sites residing at corners and edges, which are more abundant on small iron carbide particles. Lower olefins are produced at promoted (stepped) terrace sites that are available and active, quite independent of size. These results demonstrate that the iron carbide particle size plays a crucial role in the design of active and selective FTO catalysts.
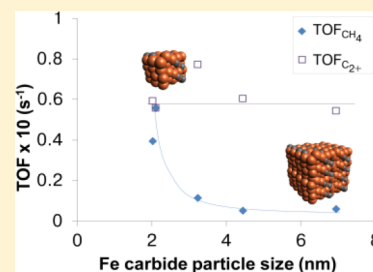
INTRODUCTION

Lower olefins (C_2−C_4) are the key building blocks of the chemical industry. These short hydrocarbons are traditionally produced by steam cracking of naphtha or as byproducts of oil refining processes. The strategic determination of several countries to decrease their dependence on imported crude oil, the rapid depletion of known oil sources, and the pressing necessity to minimize the carbon footprint have directed the research efforts into the development of alternative feedstocks and processes to produce chemicals.

The Fischer−Tropsch synthesis has long been known as an alternative process to produce long-chain hydrocarbons for their use in transportation fuels. In the Fischer−Tropsch reaction, synthesis gas produced from natural gas reforming or gasification of coal or biomass is transformed in the presence of cobalt, ruthenium, or iron catalysts. The product distribution is highly dependent on the process conditions and the type of catalyst used.

An alternative process to produce lower olefins from synthesis gas is the so-called FTO or Fischer−Tropsch to Olefins process. This reaction is carried out at more elevated temperatures (>300 °C) to shift selectivity toward short-chain hydrocarbons.[1−3] A catalyst for the selective production of C_2−C_4 olefins from synthesis gas that has been previously reported consists of iron nanoparticles dispersed on an inert support material.[1,2]

The Fischer−Tropsch reaction is recognized as a structure-sensitive reaction[4,5] which means that the catalytic performance is strongly related to the particle size of the metal or active phase. The effect of metal particle size has been extensively studied for cobalt[6−10] and ruthenium.[11−14] However, in the case of iron, the number of research studies concerning the effect of particle size is limited since iron catalysts used in the Fischer−Tropsch synthesis are often unsupported or bulk catalysts.

Park et al.[15] studied the effect of Fe particle size for unpromoted δ-Al_2O_3-supported catalysts. These catalysts showed an increase of methane selectivity with a decrease of Fe crystallite size. The turnover frequency (TOF) of Fe/δ-Al_2O_3 increased with particle size toward a maximum for catalysts with average Fe crystallite size of 6 nm and larger.

The effect of particle size of the active phase on catalytic performance might be obscured by the influence of strong metal support interactions. It is well-known that iron forms mixed oxides when supported on alumina or silica.[16] These aluminates or silicates are difficult to reduce, and the formation

of the active iron carbide phase is hindered. To study the intrinsic particle size effect and to limit support effects, it is necessary to use a carrier material with limited interaction toward iron such as carbon nanofibers.[1,2,6,7]

During the eighties, studies concerning the effect of Fe crystallite size were performed on unpromoted carbon-supported[17,18] and γ-Al$_2$O$_3$-supported catalysts.[19] Jung et al.[17] reported that, under the conditions used (1 bar, 275 °C, and H$_2$/CO = 3), smaller Fe particle sizes (<1.6 nm) lead to lower turnover frequencies for CO hydrogenation, lower methane selectivities, and higher olefin to paraffin (O/P) ratios. In a subsequent study, Jones et al.[18] found similar trends for methane selectivity and TOF with iron (carbide) particle size. However, they observed higher O/P ratios for catalysts with larger Fe particles. The discrepancy in the results was attributed to the different testing conditions used in the study of Jones et al. (1 bar, 200 °C, and H$_2$/CO = 2). In both studies, it was stated that carbon-supported catalysts are more selective to olefins in comparison with samples prepared with γ-Al$_2$O$_3$ as support.

An interesting study related to the effect of iron particle size on catalytic performance using supported and K-promoted catalysts was carried out by Barkhuizen et al.[12] The Fe particles were prepared by the reverse micelle technique and were dispersed on activated carbon or γ-Al$_2$O$_3$. The Fischer–Tropsch reaction was carried out at 270 °C, 30 bar, and H$_2$/CO = 2. For particles with average sizes smaller than 10 nm a decrease in particle size led to a decrease in surface-specific activity and chain growth probability and higher methane selectivity. The lower activity of smaller Fe particles was attributed to preferential coverage with carbon layers or to a lower density of specific sites for chain growth during the Fischer–Tropsch reaction. However, for this particular study it was difficult to discern between particle size and promoter effects.

It is noted that iron carbide is recognized as the active phase for the Fischer–Tropsch reaction and not iron in its metallic state.[18,20−23] Density functional theory (DFT) calculations have shown that metallic iron and iron carbide have distinct catalytic behaviors as they display different CO dissociation barriers and binding strengths for C and O atoms.[24−26]

The research studies concerning the Fe particle size effect for supported catalysts have been performed at relatively low temperature (~250 °C) to investigate catalysts dedicated to the production of transportation fuels and not the high temperatures (~350 °C) required for the synthesis of lower olefins.

In this study, we focused on the influence of Fe carbide particle size on catalytic performance at elevated temperatures (340−350 °C). Carbon nanofiber (CNF) supported catalysts with different iron oxide particle sizes were synthesized and tested under FTO conditions to analyze the carbide particle size effect on activity and C$_2$−C$_4$ olefins and methane selectivity. Here we have studied both promoted and unpromoted systems to decouple size effects from the influence of promoters.

■ EXPERIMENTAL METHODS

Preparation of the CNF Support. A 5 wt % Ni/SiO$_2$ catalyst was prepared by homogeneous deposition precipitation as described elsewhere.[27] An amount of 4 g of the calcined nickel catalyst, sieve fraction 150−212 μm, was placed in a tubular oven and reduced in situ under the flow of a H$_2$ (80 mL min^{-1}) and N$_2$ (320 mL min^{-1}) mixture at a pressure of 2.8 bar and 700 °C for 2 h (ramp 5 °C min^{-1}).

After reduction, the flow was switched to a mixture of CO (80 mL min^{-1}), H$_2$ (28 mL min^{-1}), and N$_2$ (292 mL min^{-1}) at a pressure of 3 bar, and the oven temperature was decreased to 550 °C. The carbon nanofibers were grown for 24 h. After growth, the product was refluxed in 200 mL of 1 M aqueous solution of KOH for 2 h to remove the silica support. After the basic treatment, the fibers were washed until neutral pH with demineralized water. Subsequently, the fibers were subjected to a treatment by refluxing in concentrated HNO$_3$ for 2 h to remove nickel and to introduce oxygen-containing groups on the surface of the fibers. After the acid treatment, the fibers were washed with demineralized water until neutral pH and dried overnight under static air at 120 °C.

Catalyst Preparation and Characterization. *Preparation of Unpromoted Supported Catalysts (Impregnation).* Five catalysts with different iron loadings (1, 2, 5, 10, and 20 wt % Fe) were prepared by incipient wetness impregnation of aqueous solutions of ammonium iron citrate (Fluka, purum p.a., 14.5−16 wt % Fe) on oxidized CNF (150 m^2 g^{-1}, pore volume 0.5 mL g^{-1}). In the case of the 1 and 2 wt % Fe catalysts, the pore volume of the support was filled with the total volume of the solution in a single step. For the other samples, it was necessary to carry out successive impregnations. Between impregnation steps the samples were dried under static air at 120 °C for 1 h. After total usage of the solution, the samples were dried overnight under static air at 120 °C. In a subsequent step, the impregnated and dried samples were heat treated under nitrogen in a plug flow reactor at 500 °C for 2 h (5 °C min^{-1}; 150 mL min^{-1} for 150 mg of precursor loaded catalyst). The samples were cooled to room temperature and were passivated by oxidation with diluted oxygen. The oxygen concentration was increased stepwise (2% v/v increase every 30 min) until reaching 20% v/v. The number in the sample code indicates the nominal iron loading. IM means that the sample was prepared by impregnation and did not contain promoters.

Preparation of Unpromoted Supported Catalysts (Colloidal Synthesis). Three catalysts with different iron oxide particle sizes were prepared by using a colloidal synthesis based on the thermal decomposition of iron oleate. The iron complex was prepared according to the procedure described by Bronstein et al.[28] An amount of 1.08 g of iron oleate was mixed with 1.24 mL of oleic acid, 13 mL of the solvent (hexadecene, octadecene, or docosane, depending on the desired particle size), and 2 g of surface-oxidized carbon nanofibers (150 m^2 g^{-1}) to achieve a nominal iron loading of 10 wt %. The mixture was heated to the boiling temperature of the solvent (275, 315, 370 °C, respectively) with a heating ramp of 3.3 °C min^{-1} and was kept at the final temperature for 30 min. After cooling to room temperature, the supported catalysts were washed three times with a mixture of hexane and acetone (1:4 volumetric ratio). The solids were separated by filtration and dried under vacuum at 40 °C in a rotary evaporator for 1 h. The dried catalysts were heat treated under nitrogen flow at 350 °C for 2 h (ramp 10 °C min^{-1}, 150 mL min^{-1} for 150 mg of precursor loaded catalyst). The number in the sample codes indicates the nominal iron loading. The letters provide information about the preparation method: CH, colloidal hexadecene; CO, colloidal octadecene; CD, colloidal docosane.

Preparation of Promoted Supported Catalysts. Five catalysts with different iron loadings (1, 2, 5, 10, and 20 wt % Fe) were prepared as described above by incipient wetness impregnations of aqueous solutions of ammonium iron citrate (J. T. Baker, 14.5−16 wt % Fe, Na, S: ~ 750 mg kg^{-1}) on oxidized CNF. This iron precursor contained traces of sodium and sulfur which are suitable promoters for FTO.[1,29,30] The preparation procedure was as described for the unpromoted catalysts synthesized with the impregnation technique. The sample code is similar as previously explained for unpromoted samples prepared by impregnation. To differentiate between unpromoted and promoted samples, a letter P was added to the sample code of promoted catalysts.

Fresh and Spent Catalyst Characterization. Iron loadings of samples prepared by colloidal synthesis were measured with X-ray fluorescence (XRF) on a Goffin Meyvis Spectro X-lab 2000 machine. The average crystallite size of the iron oxide particles was determined by analysis of the line broadening in the X-ray diffraction (XRD)

Table 1. Properties of Unpromoted CNF-Supported Iron Catalysts

sample	preparation	Fe loading (wt %)	Fe$_2$O$_3$ crystallite size; XRD (nm)	Fe$_2$O$_3$ particle size (nm)^c	Fe$_5$C$_2$ particle size (nm)^d	Fe particle size (nm)^d
1IM	impregnation	1^a	–	2.6	2.1	2.0
2IM	impregnation	2^a	–	2.5	2.0	1.9
5IM	impregnation	5^a	–	4.0	3.2	3.1
10IM	impregnation	10^a	7	5.5	4.4	4.3
20IM	impregnation	20^a	10	8.6	6.9	6.7
10CH	colloidal	8^b	7	8.1	6.5	6.3
10CO	colloidal	8^b	11	14.2	11.5	11.0
10CD	colloidal	12^b	17	16.9	13.6	13.1

^{a}Nominal iron loading. ^{b}Iron loading measured with XRF. ^{c}Number average determined by TEM analysis. ^{d}Calculated from TEM data of Fe$_2$O$_3$.

patterns recorded at room temperature. The measurements were performed with a Bruker AXS D8 Advance diffractometer equipped with a Co$_{K\alpha,1}$ source (λ = 0.178897 nm) from 25° to 80° in 2θ. The distribution of iron oxide on the support and the particle size distribution were obtained by the analysis of transmission electron microscopy (TEM) micrographs. The images were acquired on a Philips Tecnai-20 FEG (200 kV) microscope equipped with an EDX and HAADF detector. The composition of the Fe phase before reaction, after reduction, and after FTO reaction was determined in situ with transmission ^{57}Fe Mössbauer spectroscopy. The spectra were collected at room temperature with a conventional constant acceleration spectrometer using a ^{57}Co (Rh) source. Velocity calibration was carried out using an α-Fe foil. The Mössbauer parameters were estimated by fitting the spectra using the Mosswin 3.0i program.

Catalytic Tests. *Low Pressure Testing.* The Fischer−Tropsch synthesis was performed at 1 bar and 250 or 350 °C using a mixture of H$_2$ and CO (1/1 v/v). H$_2$ (99,999%), CO (99%), and Ar (99,999%) were supplied by Linde Gas and used without further purification. An amount of 20 mg of the catalyst (particle size 0.2−0.4 mm, ρ = 0.55 g mL^{-1}) was diluted with 200 mg of SiC (particle size 0.2 mm) and placed in a plug flow reactor. The reaction was carried out at low CO conversions (<1%) to ensure differential operation. When the Fischer−Tropsch reaction was performed at 250 °C, the catalysts were reduced in situ, prior to reaction, using a mixture of H$_2$ and Ar (33% v/v H$_2$; 60 mL min^{-1}) at 350 °C for 2 h (ramp 5 °C min^{-1}). In the case that the reaction was carried out at 350 °C, the catalysts were heated under Ar flow until the reaction temperature (ramp 5 °C min^{-1}). Subsequently, the flow was switched to the H$_2$/CO mixture (6 mL min^{-1}). The effect of pretreatment on catalytic performance (reduction under H$_2$ or direct activation under syngas) was negligible for samples tested at 350 °C and 1 bar. The product selectivity to hydrocarbons up to C$_{16}$ was determined with gas chromatography using a Varian CP3800 analyzer equipped with an FID detector (Column CP Sil 5 CB). The GC was calibrated with a gas mixture of known composition. The calibration for low concentrations was performed by dilution of the calibration mixture to ensure the reliability of the data at low CO conversions. CO$_2$ selectivity was not measured. The product selectivity was calculated on a carbon atom basis: (moles of product Y) × (carbon atoms in product Y)/(total carbon atoms in hydrocarbons produced). The catalytic activities expressed as moles of CO converted to hydrocarbons per gram of iron per second (FTY) or per mole of surface sites per second (TOF) were determined after 1 and 15 h of reaction. Apparent TOF was calculated using the density of Fe$_5$C$_2$ (ρ = 7.57 g mL^{-1}) and assuming 14 Fe atoms nm^{-2}. It has been assumed that the iron-containing particles consist fully of iron carbide at their surfaces. The selectivity to oxygenates was below 1%C$_{at}$ and therefore excluded.

Medium Pressure Testing. The Fischer−Tropsch synthesis was carried out in a plug flow reactor at 20 bar and 340 °C using a mixture of H$_2$ and CO (1/1 v/v) with a space velocity of 3000 h^{-1}. CO (99.9%), H$_2$ (99.95%), N$_2$ (99.996%), and He (99.9992%) supplied by Praxair were used and further purified for sulfur and carbonyls with a Vici Metronics T400-2 trap. An amount of 100 μL of catalyst (particle size 0.2−0.4 mm, ρ = 0.55 g mL^{-1}) was diluted with SiC (particle size 0.2−0.4 mm) to complete a volume of 200 μL. The catalysts were

reduced in H$_2$ at 350 °C for 2 h prior to reaction. The initial CO conversion was in the range of 23−89% for the promoted catalysts. The product selectivity to hydrocarbons up to C$_9$ was determined with online gas chromatography and was calculated on a carbon atom basis. The analysis of the gases was performed using a Siemens Maxum II analyzer for parallel chromatography equipped with Restek CHR-PAW, Agilent GS-GasPro, Restek MXT1 columns. The catalytic activities and selectivities reported here were determined at the start of the Fischer−Tropsch reaction (1 h). The liquid products were collected in a hot trap, and the composition of the cumulative liquid was analyzed offline with GC × GC on an Agilent 7890 machine equipped with Agilent DB-17 and CP-Sil5 columns. The analysis confirmed the production of hydrocarbons in the range of C$_8$ to C$_{15}$. Trace amounts of alcohols, mainly ethanol, were observed. CO$_2$ selectivities were determined too. A blank experiment in which heat-treated CNF (heat treatment at 750 °C to expose encapsulated nickel particles) were tested under FTO conditions showed negligible activity for methanation, and thus contributions on activity and selectivity by methane formation due to the presence of possible nickel traces in the CNF support were ruled out.

■ RESULTS AND DISCUSSION

The analysis of TEM images of unpromoted catalysts prepared by the incipient wetness impregnation (IWI) method demonstrated that different iron oxide particle sizes were obtained at different iron loadings. Nominal or apparent iron carbide (χ-Fe$_5$C$_2$) particle sizes were calculated from the average Fe$_2$O$_3$ particle sizes determined with TEM analysis. Here we report our results in relation to iron carbide sizes instead of referring to metallic Fe since Hägg carbide, Fe$_5$C$_2$, has been suggested to be the active phase during the Fischer−Tropsch reaction.[21,24,31] The estimated carbide sizes are smaller than measured Fe$_2$O$_3$ sizes and similar to calculated Fe sizes in view of density differences (Table 1).

In the case of the samples synthesized with the IWI technique, iron carbide particle size increased as a function of iron loading (Table 1, Figure S1, Supporting Information). The Fe$_2$O$_3$ particle sizes reported in Table 1 and Figure S1 (Supporting Information) correspond to unpromoted catalysts. TEM analysis of selected promoted samples demonstrated that average iron oxide particle sizes were identical for unpromoted and promoted catalysts prepared by the IWI preparation method. Figure 1 shows that the particle size distribution for the 2 and 5 wt % Fe samples prepared by impregnation is narrow.

The standard deviation from the average diameter was approximately 23%. Broader distributions were observed for the 1 wt % Fe catalyst and samples with higher iron loadings (Figure S2, Supporting Information). TEM analysis of catalysts prepared by colloidal synthesis showed that these samples had a relatively narrow size distribution. A typical TEM image of a catalyst (10CO) prepared using octadecene as solvent is shown
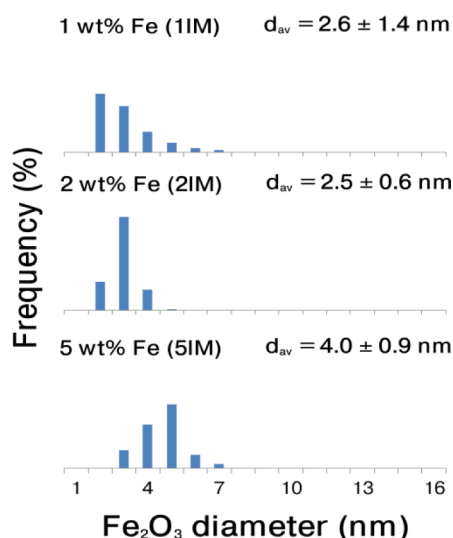
Figure 1. Particle size distribution of iron oxide from TEM analysis of unpromoted catalysts prepared by incipient wetness impregnation revealed narrow size distributions of Fe_2O_3 particles for the 2 wt % Fe/CNF and 5 wt % Fe/CNF samples.

in Figure 2. The histograms from the particle size distribution analysis of catalysts prepared with colloidal synthesis are included in Figure S2 (Supporting Information).
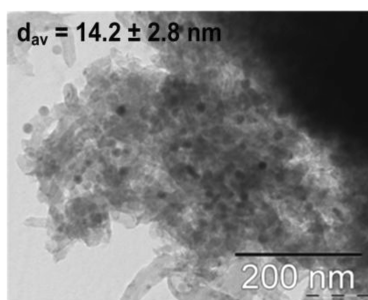

Figure 2. TEM image of a catalyst (10CO) prepared by colloidal synthesis. The Fe_2O_3 particles were homogeneously dispersed on the carbon nanofibers and had a narrow size distribution when the samples were prepared by thermal decomposition of iron oleate in octadecene.

Analysis of diffraction patterns measured with XRD showed that Fe_2O_3 line broadening was only observable on samples with crystallite sizes larger than 4 nm due to technique and equipment limitations (Table 1). The Fe_2O_3 crystallite sizes measured with XRD analysis are in close agreement with the particle sizes determined with TEM. The iron loadings, number-average Fe oxide sizes, and the calculated carbide sizes are displayed in Table 1.

Promoted and unpromoted Fe/CNF catalysts were tested at 250 and 350 °C for the Fischer−Tropsch reaction to determine (1 bar, H_2/CO = 1 v/v) the effect of iron carbide particle size at 250 and 350 °C. The catalysts were tested under low CO conversion (<1%) to ensure differential operation. Most of the samples showed deactivation probably caused by carbon deposition under low pressure and low H_2/CO ratio conditions. Deactivation due to carbon deposition during the FTO reaction at low H_2/CO ratios was previously observed by Sommen et al.[32] for Fe/AC and by Koeken et al.[33] for Fe/α-Al_2O_3 catalysts. The catalytic activity as a function of time on stream for promoted and unpromoted samples at 250 and 350

°C conditions is included in the Supporting Information (Figure S3).

The catalytic results at 1 bar of unpromoted and promoted samples showed that the catalytic activity per gram of iron (iron time yield, FTY) increased with the decrease of Fe_5C_2 particle size regardless of reaction temperature (Figure 3, 350 °C and
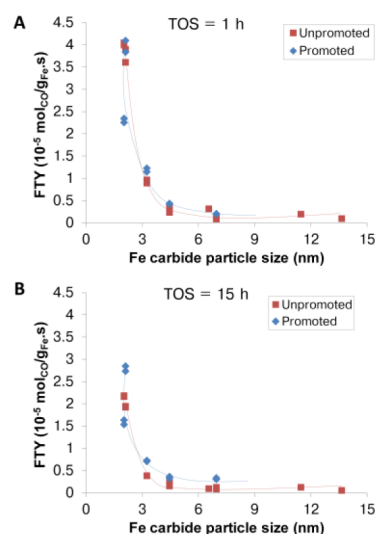

Figure 3. Iron time yield (FTY) as a function of particle size. The iron-normalized activity of Fe/CNF catalysts (unpromoted ■; promoted ◆) decreased with an increase in iron particle size. A, TOS = 1 h; B, TOS = 15 h. The reaction was performed at 350 °C, 1 bar, and H_2/CO = 1 v/v.

Figure S4, Supporting Information, 250 °C). This effect was most pronounced for iron carbide particles smaller than 4 nm. Figure 3A shows FTY determined after 1 h of reaction, while Figure 3B displays the catalytic activities after 15 h of reaction. From these plots it is observed that the increase of catalytic activity with the decrease of particle size was maintained after 15 h of reaction despite more severe deactivation for smaller particles (Figure S3, Supporting Information). TEM analysis of selected samples evidenced that after reaction at 1 bar the iron-containing particles experienced limited levels of sintering (Table S1, Supporting Information).

Our results on catalytic activity show an opposite trend compared to the results reported by other research groups for iron catalysts supported on activated carbon or δ- and γ-Al_2O_3. In these studies the effect of metal−support interactions might have masked the influence of Fe particle size, even in the case of activated carbon.[18] A comparative experiment evidenced that a promoted Fe/AC catalyst (Table S2, Supporting Information) prepared by impregnation of ammonium iron citrate had an FTY five times lower compared to a promoted Fe/CNF catalyst with a similar Fe particle size. Mössbauer spectroscopy suggested that the Fe/AC catalyst had a lower degree of carbidization and a concomitant higher amount of Fe(II) oxide.

The higher FTY observed for catalysts with smaller Fe_5C_2 particle sizes might be attributed to a lower extent of carbon deposition and thereby deactivation. However, activity trends are similar for short and longer times on stream (Figure 3).

Additional characterization experiments using in situ Mössbauer spectroscopy (1 bar, 350 °C, H_2/CO ratio of 1 v/v, TOS = 15 h) indicated that catalysts with different iron carbide particle sizes before reaction (2.0 and 4.4 nm, respectively) exhibited different degrees of carbidization and

Table 2. Catalytic Activity and Product Selectivity under FTO Conditions of Promoted and Unpromoted Fe/CNF (1 bar, 350 °C, H_2/CO = 1, TOS = 15 h) of Fe/CNF Catalysts

sample	FTY (10^{-5} mol_{CO}/g_{Fe} s)	apparent $TOF^a \times 10^3$ (s^{-1})	product selectivity (%C_{at}, CO_2-free)			
			CH_4	C_2–C_4 olefins	C_2–C_4 paraffins	C_{5+}
1IM	1.93	10.9	40	49	5	6
2IM	2.19	11.9	45	46	3	6
5IM	0.39	3.4	36	50	3	11
10IM	0.16	1.9	34	51	3	12
20IM	0.09	1.7	36	49	3	12
10CH	0.10	1.5	38	54	3	5
10CO	0.13	3.1	37	50	2	11
10CD	0.06	2.2	48	47	2	3
1IMP	2.74	15.5	41	49	4	6
2IMP	1.64	8.9	37	51	5	7
5IMP	0.73	6.3	33	52	7	8
10IMP	0.37	4.4	28	57	5	10
20IMP	0.31	5.2	20	65	2	13
$2IMDP^b$	2.68	14.6	36	52	6	6

^{a}Apparent turnover frequency: moles of CO converted to hydrocarbons per mole of surface Fe_5C_2 per second. ^{b}Sample prepared with an additional amount of Na and S

(Table S3, Supporting Information). The higher activity of 10IMP compared with 10IM could be ascribed to higher total carbidic content (Fe_xC (SPM) plus Fe_5C_2). However, samples with similar total carbide contents exhibited different catalytic performance (comparison between 2IM and 10IM or between 2IMP and 10IMP). This result suggests that two iron-containing particles having approximately the same composition, but different sizes displayed a dissimilar catalytic behavior probably because of differences in the nature and number of active sites.

The results of the catalytic tests of unpromoted and promoted catalysts under FTO conditions (350 °C) are further summarized in Table 2. We have assumed that the active particles fully consist of iron carbide at their surface as suggested by HR-TEM studies of Datye and co-workers.[34] Nevertheless, it is acknowledged that iron oxide might be present on the surface of the Fe-containing particles in the case of carbide reoxidation, as observed in previous studies at high CO conversions.[35] This assumption implies that the calculated TOF values have to be considered as lower limits and will be referred to as "apparent TOF" in the text and figures. The apparent TOF data presented in Table 2 correspond to initial activities (after 1 h of reaction). Methane and C_2–C_4 olefin selectivities are also plotted as a function of Fe_5C_2 size in Figure 4.

The effect of iron carbide size on product selectivity was almost nil for unpromoted catalysts, although some scatter was apparent for the smallest and largest sizes (Figure 4A). These catalysts exhibited a fairly high selectivity toward lower olefins (~50%C_{at}) in combination with a high methane production (~40%C_{at}). The samples with the lowest methane selectivity displayed slightly lower C_2–C_4 olefins selectivities (~47%).

In contrast to the behavior observed for unpromoted catalysts, the product selectivities of promoted Fe/CNF samples exhibited a clear effect of iron carbide particle size (Figure 4B). Lower olefin selectivity increased from 50%C_{at} to 65%C_{at}, while CH_4 selectivity showed an opposite trend decreasing from 40%C_{at} to 20%C_{at} when Fe_5C_2 size increased from 2 to 7 nm.

The Anderson–Schulz–Flory (ASF) plots for the promoted catalysts are shown in Figure S5 (Supporting Information). For
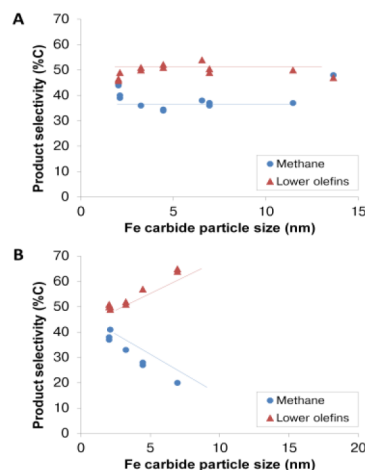

Figure 4. Product selectivity as a function of particle size. Selectivity toward methane and lower olefins of Fe/CNF catalysts: (A) unpromoted and (B) promoted. Product selectivity: C_2–C_4 olefins (▲) and methane (●) (reaction conditions: 1 bar, 350 °C, H_2/CO = 1, TOS, 15 h).
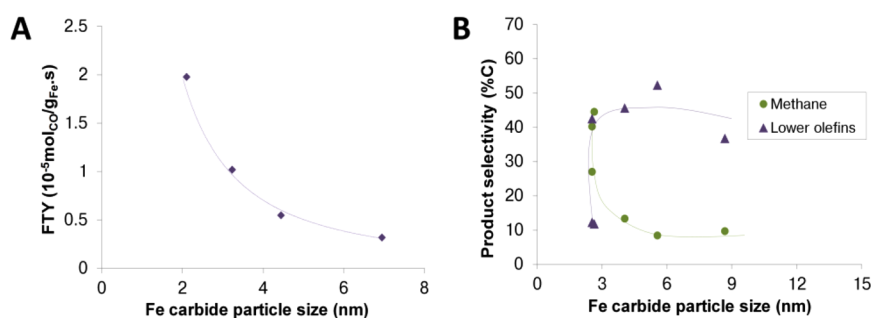
these samples, it was observed that chain growth probability (α) increased with particle size. The samples with the smallest iron carbide sizes (1IMP, 2IMP) followed the ASF product distribution, while larger particles (5IMP, 10IMP) showed methane selectivities below the values predicted by the model.

This remarkable selectivity response for promoted catalysts cannot be attributed to an intrinsic particle size effect of iron carbide since the results of the unpromoted catalysts confirmed that the influence of iron carbide size on product selectivity was minimal (Figure 4A). The increase of lower olefin selectivity and the decrease of CH_4 production with the increase of Fe_5C_2 particle size might be ascribed to higher coverages of promoters on the active surface for larger sizes.

The fact that unpromoted and promoted catalysts with small Fe_5C_2 sizes (~2 nm) exhibited similar product selectivities possibly confirms this explanation. An additional experiment was performed introducing additional Na and S during the synthesis of the catalyst 2IMDP to achieve a double amount of promoters compared with sample 2IMP. Results of the catalytic

Table 3. Catalytic Performance of Promoted and Unpromoted Fe/CNF under FTO Conditions (20 bar, 340 °C and H_2/CO = 1, TOS = 1 h)

sample	CO conv. (%)	CO_2 (%CO conv.)	FTY (10^{-4} mol $_{CO}$/g$_{Fe}$ s)	Apparent TOF × 10 (s^{-1})	product selectivity (%C$_{at}$, CO_2-free)				
					CH_4	C_2–C_4 olefins	C_2–C_4 paraffins	C_{5+}	Oxyg.
1IM	10	35	1.42	0.8	57	6	34	2	2
2IM	9	32	0.38	0.2	34	13	46	7	0
5IM	11	46	0.20	0.2	27	17	45	12	0
10IM	11	46	0.13	0.2	59	4	34	0	3
20IM	10	42	0.06	0.1	43	21	32	0	3
1IMP	12	38	1.98	1.1	50	6	34	1	9
2IMP	30	46	1.82	1.0	40	12	41	1	5
5IMP	82	49	1.02	0.9	13	46	32	6	3
10IMP	86	47	0.55	0.7	8	52	7	28	5
20IMP	87	42	0.32	0.6	10	37	23	28	2

Figure 5. Catalytic performance of promoted catalysts at medium pressure (340 °C, 20 bar, and H_2/CO = 1). (A) The catalytic activity per gram of iron (FTY) of promoted Fe/CNF catalysts. (B) Product selectivity: methane (●) and C_2–C_4 olefin (▲) selectivities show an opposite trend with the increase of iron particle size.

test of sample 2IMDP (Table 2) indicated that the addition of extra amounts of promoters did not affect product selectivity, although it gave rise to an enhanced catalytic activity. This result might suggest that small iron carbide particles have a large number of sites for CH_4 formation that might be difficult to affect with sodium/sulfur.

Promoted and unpromoted catalysts prepared by impregnation were tested under FTO conditions at medium pressure (20 bar) to assess the effect of iron carbide particle size on catalytic performance at industrially relevant conditions. The results summarized in Table 3 were measured after 1 h time on stream after which limited sintering as well as limited coke lay-down[33] is expected.

In the case of unpromoted catalysts, a decrease in FTY and apparent TOF was observed with an increase in iron carbide particle size, similarly to the behavior observed when the reaction was performed at 1 bar. The C_2–C_4 olefin selectivity for these catalysts was low (<20%C$_{at}$) and accompanied by high methane production (>30%C$_{at}$) (Table 3).

The activity per gram of iron (FTY) and apparent turnover frequency for promoted catalysts also decreased with an increase of Fe_5C_2 particle size as shown in Table 3. The activity of the promoted catalysts was almost five times higher than for unpromoted catalysts with the same iron carbide sizes, with the exception of sample 1IMP. A similar trend for the catalytic activity as a function of the Fe_5C_2 particle size is observed when performing the FTO reaction under low (Figure 3) and medium pressures (Figure 5), although at the latter condition FTYs were five to fifteen times higher.

For the promoted catalysts also at 20 bar, lower olefins selectivity increased with the increase of iron carbide size, albeit that for the sample with the largest particle size (~7 nm) a

somewhat lower selectivity was observed (Figure 5B). From the results of the catalytic tests, it is apparent that C_{5+} selectivity also increased when particle size increased (Table 3). A different behavior at 20 bar was also observed for methane where selectivity was high for small particle sizes (~2 nm), but it did not decrease any further with the increase of Fe_5C_2 size, setting a limit around 10%C$_{at}$ (Figure 5B).

Analysis of TEM images of spent samples indicated that iron-containing particles had sintered during reaction at 20 bar. Figure 6 shows micrographs of two spent promoted Fe/CNF
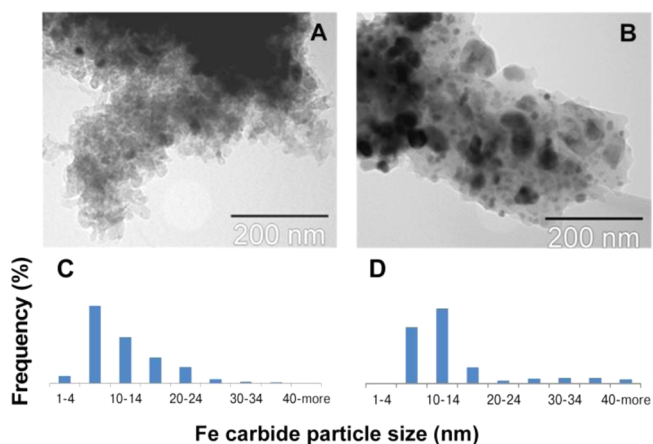
Figure 6. TEM of spent promoted samples after FTO at 340 °C, 20 bar, and H_2/CO = 1, TOS = 40 h. (A) Sample 5IMP with average particle size of 3 nm before reaction and (B) sample 20IMP with particle size of 7 nm before reaction. Histograms of the iron carbide sizes after reaction: (C) sample 5IMP and (D) sample 20IMP.

catalysts and their respective particle size distribution. The average carbide size for the spent catalyst 5IMP was 11.1 ± 6.4 nm, while for the catalyst 20IMP the average size after reaction was 13.5 ± 9.5 nm. From these results, it is observed that a sample with a small initial particle size suffered a higher extent of sintering compared to a sample with a larger size. Activity plots as a function of time on stream (Figure S6, Supporting Information) indicated that catalysts with smaller carbide sizes indeed deactivated faster than samples with larger Fe_5C_2 sizes.

Due to the carbonaceous nature of the support, it is difficult to distinguish the carbon deposited during reaction. For this reason, in future work we propose to perform in situ carbon lay-down measurements. Tentatively, for the catalysts with small particle sizes the fast deactivation is attributed to loss in active surface area caused by sintering rather than carbon lay-down.

■ GENERAL DISCUSSION AND CONCLUSIONS

Carbon nanofiber supported iron (carbide) particles in the range from 2 to 17 nm have been synthesized. For promoted and unpromoted catalysts at low pressure (1 bar) and medium pressure (20 bar), the initial surface-specific activities (apparent TOF) for total hydrocarbons produced increased with decreasing particle size. For example, the apparent TOF of the CO conversion to hydrocarbons (340 °C, 20 bar) of promoted catalysts increased from 0.06 to 0.11 s^{-1} when the iron carbide particle size decreased from 7 to 2 nm (Figure 7).
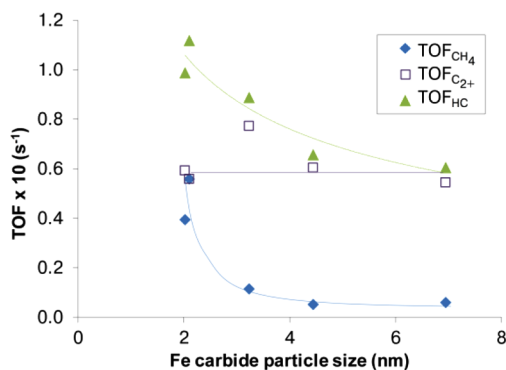

Figure 7. Apparent turnover frequencies (TOF) as a function of iron carbide size (TOS = 1 h). TOF_{HC} and TOF_{C2+} correspond to the CO conversion to hydrocarbons and conversion to C_{2+} hydrocarbons, respectively. The reaction was performed at 340 °C, 20 bar, and a H_2/CO ratio of 1 (v/v) on promoted catalysts.

Although we realize that the TOF values of our catalysts cannot be calculated with the same accuracy as for metal catalysts (no direct way of measuring the number of active sites is available), the difference of apparent TOF values is quite large, and trends are meaningful in our opinion. The apparent TOF data discussed here correspond to initial activities. It is important to realize that the effect of particle size on specific surface activity is different when the surfaces are relatively clean (initial state) from those after the reaction has proceeded for longer times and the iron-containing particles have sintered or have been covered with amorphous or graphitic carbon (steady state). Values of apparent TOF at steady state for selected samples are shown in Table S4 (Supporting Information). After 40 h of reaction, the apparent TOF trend changed, increasing through a maximum (sample 5IMP) with decreasing the average carbide size. The apparent TOFs based on initial activities are crucial to

understand the fundamental surface processes, and they can more easily be related to theoretical studies on clean surfaces. The values of TOF at steady state are useful to understand the processes occurring at the surface of a working catalyst and the corresponding deactivation mechanisms.

The trend observed with Fe is in stark contrast with previous results for Co as well as Ru. For these metals TOF dropped significantly below a certain critical particle size. For cobalt this has been assigned to combined effects of poisoning of low coordination sites at corners and edges by strongly bonded CO and a lower fraction of active step edge sites at terraces of particles smaller than 6 nm.[7] Clearly, iron carbide nanoparticles display vastly different size effects, and it should be realized that the nature of chemical bonding in metal carbide is different from a metal. Here we put forward that corners and edges of iron carbide nanoparticles display high activity in particular to produce methane, while terraces of the particles are not much affected by size. This proposal is based on the analysis of apparent TOF for different product fractions (Figure 7). The TOF for the production of C_{2+} hydrocarbons is independent of size, whereas the TOF for methane formation increases sharply for particles smaller than 4 nm.

On the basis of DFT calculations, Cheng et al.[24] have proposed a volcano-plot for M—C bond strength versus FT activity for Co and Fe. They have linked the higher activity of Fe carbide over Fe metal to weaker Fe—C bond strength of the carbide phase. From their plot, it is suggested that further weakening of the Fe—C bond in iron carbide would further enhance activity. Our particle size effect suggests even weaker Fe—C bonds at corners and edges of iron carbide nanoparticles, thereby enhancing the overall TOF, albeit mainly by enhanced methane formation.

The concept of the Fe—C bond strength also gives further insight into activity differences between Na plus S promoted and unpromoted catalysts. For promoted catalysts the higher TOF is tentatively explained by sulfur that weakens Fe—C bonds, thereby enhancing FT activity. Please note that addition of extra Na + S promoters did not affect selectivity but enhanced activity further (2IMP versus 2IMDP, Table 2).

Selectivity differences between catalysts should be considered with care in the case of large conversion differences between catalysts (20 bar, Table 3) in view of possible different extents of secondary reactions. Since the experiments at 1 bar have all been carried out at low CO conversion levels (<1%), we may use these data with more confidence. From the selectivity data obtained at 1 bar and summarized in Figure 4A, it appears that for unpromoted catalysts methane selectivity as well as C_2–C_4 olefin selectivity are both high and independent of particle size. It is put forward that for unpromoted iron carbide low coordination sites at corners and edges and sites at terraces are similar in terms of selectivity but not in terms of activity since the former are more active and give rise to the particle size effect on apparent TOF discussed above. Figure 4B shows for promoted catalysts significant effects of iron carbide particle size on selectivity. For the smallest promoted particles of 2 nm, the selectivities are very similar to those of unpromoted particles, whereas olefin selectivities increase and methane selectivities decrease for larger particles. Sulfur (possibly anchored by sodium) on the surface of larger iron carbide particles suppresses methane selectivity and enhances lower olefin selectivity to a large extent. The promoters are not effective with small particles, tentatively explained by that only terraces of nanoparticles are affected and not corners and edges.

Since corners and edges dominate activity for the smallest particles, selectivities of promoted and unpromoted particles converge (Figures 4A and 4B).

The medium pressure results summarized in Figure 7 nicely display the overall effects of activity and selectivity. In view of the similar results obtained at 1 bar we can also quantitatively interpret the trends for these results. Large particles are effectively promoted by Na plus S, thus displaying low methane selectivities that are below predictions from Anderson–Schulz–Flory distribution as discussed in reference 1 and confirmed in Figure S5 (Supporting Information). Sulfur might be effective in lowering hydrogen coverage on iron carbide thereby suppressing chain termination by hydrogenation and thus methane formation. From figure 7 it appears that for a short time on stream, TOF for methane increased for promoted catalysts much more strongly (∼ factor of 10) than the overall TOF (∼ factor of 2). Also note from Table 2 (1 bar) and Table 3 (20 bar) that TOF enhancements with decreasing particle sizes are much larger for unpromoted catalysts than for promoted catalysts. We propose that sulfur/sodium enhance activity and selectivity of terraces independent of size. Methane production on low coordination sites may be further enhanced by the promoters without boosting olefin selectivity for the smallest particle sizes.

In summary, we report very significant particle size (2−17 nm) effects for supported iron carbide catalysts used for the direct production of lower olefins from synthesis gas. Smaller iron carbide particles display higher surface specific activities mainly due to higher methane production. It appears that the particle size effects of Fe under the studied reaction conditions deviate from those reported earlier for Co[6−10] and Ru[11−14] and Fe[12,17,18] under low temperature Fischer−Tropsch conditions. Future studies are advocated involving surface coverages,[7] carbon lay-down,[33] and chemical bonding[21,24−26] as a function of iron carbide particle size.

ASSOCIATED CONTENT

ⓢ Supporting Information

Average carbide sizes and particle size distributions, catalytic data at 250 °C, activity as a function of time, Anderson−Schulz−Flory plots, and in situ Mössbauer parameters (Figures S1−S6, Tables S1−S5). This material is available free of charge via the Internet at http://pubs.acs.org.

AUTHOR INFORMATION

Corresponding Author
k.p.dejong@uu.nl
Notes
The authors declare no competing financial interest.

ACKNOWLEDGMENTS

REFERENCES

(1) Torres Galvis, H. M.; Bitter, J. H.; Khare, C. B.; Ruitenbeek, M.; Dugulan, A. I.; de Jong, K. P. *Science* **2012**, *335*, 835−838.
(2) Schulte, H. J.; Graf, B.; Xia, W.; Muhler, M. *ChemCatChem* **2012**, *4*, 350−355.
(3) Schwab, E.; Weck, A.; Steiner, J.; Bay, K. *Oil Gas Eur. Mag.* **2010**, *1*, 44−47.
(4) Boudart, M.; McDonald, A. *J. Phys. Chem.* **1984**, *88*, 2185−2195.
(5) van Santen, R. A. *Acc. Chem. Res.* **2009**, *42*, 57−66.
(6) Bezemer, G. L.; Bitter, J. H.; Kuipers, Herman, P. C. E.; Oosterbeek, H.; Holewijn, J. E.; Xu, X.; Kapteijn, F.; van Dillen, A. J.; de Jong, K. P. *J. Am. Chem. Soc.* **2006**, *128*, 3956−3964.
(7) den Breejen, J. P.; Radstake, P. B.; Bezemer, G. L.; Bitter, J. H.; Frøseth, V.; Holmen, A.; de Jong, K. P. *J. Am. Chem. Soc.* **2009**, *131*, 7197−7203.
(8) Prieto, G.; Martínez, A.; Concepción, P.; Moreno-Tost, R. *J. Catal.* **2009**, *266*, 129−144.
(9) Borg, Ø.; Dietzel, P. D. C.; Spjelkavik, A. I.; Tveten, E. Z.; Walmsley, J. C.; Diplas, S.; Eri, S.; Holmen, A.; Rytter, E. *J. Catal.* **2008**, *259*, 161−164.
(10) Ma, W.; Jacobs, G.; Sparks, D. E.; Gnanamani, M. K.; Pendyala, V. R. R.; Yen, C., H.; Klettinger, J. L. S.; Tomsik, T. M.; Davis, B. H. *Fuel* **2011**, *90*, 756−765.
(11) Iglesia, E.; Soled, S. L.; Fiato, R. A. *J. Catal.* **1992**, *137*, 212−224.
(12) Barkhuizen, D.; Mabaso, E. I.; Viljoen, E.; Welker, C.; Claeys, M.; van Steen, E.; Fletcher, J. C. Q. *Pure Appl. Chem.* **2006**, *78*, 1759−1769.
(13) Kang, J.; Zhang, S.; Zhang, Q.; Wang, Y. *Angew. Chem., Int. Ed.* **2009**, *48*, 2565−2568.
(14) Kellner, C. S.; Bell, A. T. *J. Catal.* **1982**, *75*, 251−261.
(15) Park, J. Y.; Lee, Y. J.; Khanna, P. K.; Jun, K. W.; Bae, J. W.; Kim, Y. H. *J. Mol. Catal. A* **2010**, *323*, 84−90.
(16) Wielers, A. F. H.; Kock, A. J. H. M.; Hop, C. E. C. A.; Geus, J. W.; van der Kraan, A. M. *J. Catal.* **1989**, *117*, 1−18.
(17) Jung, H. J.; Walker, P. L., Jr.; Vannice, M. A. *J. Catal.* **1982**, *75*, 416−422.
(18) Jones, V. K.; Neubauer, L. R.; Bartholomew, C. H. *J. Phys. Chem.* **1986**, *90*, 4832−4839.
(19) Rameswaran, M.; Bartholomew, C. H. *J. Catal.* **1989**, *117*, 218−236.
(20) Li, S.; Ding, W.; Meitzner, G. D.; Iglesia, E. *J. Phys. Chem. B* **2002**, *106*, 85−91.
(21) Shroff, M. D.; Kalakkad, D. S.; Coulter, K. E.; Köhler, S. D.; Harrington, M. S.; Jackson, N. B.; Sault, A. G.; Datye, A. K. *J. Catal.* **1995**, *156*, 185−207.
(22) de Smit, E.; Cinquini, F.; Beale, A. M.; Safonova, O. V.; van Beek, W.; Sautet, P.; Weckhuysen, B. M. *J. Am. Chem. Soc.* **2010**, *132*, 14928−14941.
(23) de Smit, E.; Swart, I.; Creemer, J. F.; Hoveling, G. H.; Gilles, M. K.; Tyliszczak, T.; Kooyman, P. J.; Zandbergen, H. W.; Morin, C.; Weckhuysen, B. M.; de Groot, F. M. F. *Nature* **2008**, *456*, 222−225.
(24) Cheng, J.; Hu, P.; Ellis, P.; French, S.; Kelly, G.; Lok, C. M. *J. Phys. Chem.* **2010**, *114*, 1085−1093.
(25) Gracia, J. M.; Prinsloo, F. F.; Niemantsverdriet, J. W. *Catal. Lett.* **2009**, *133*, 257−261.
(26) Cao, D. B.; Zhang, F. Q.; Li, Y. W.; Jiao, H. *J. Phys. Chem. B* **2004**, *108*, 9094−9104.
(27) van der Lee, M. K.; van Dillen, A. J.; Geus, J. W.; de Jong, K. P.; Bitter, J. H. *Carbon* **2006**, *44*, 629−637.
(28) Bronstein, L. M.; Huang, X.; Retrum, J.; Schmicker, A.; Pink, M.; Stein, B. D.; Dragnea, B. *Chem. Mater.* **2007**, *19*, 3624−3632.
(29) Bromfield, T. C.; Coville, N. J. *Appl. Catal., A* **1999**, *186*, 297−307.
(30) Crous, R.; Bromfield, T. C.; Booyens, S. International Publication No. WO 2010/066386, 2010.
(31) Luo, M.; Hamdeh, H.; Davis, B. H. *Catal. Today* **2009**, *140*, 127−134.
(32) Sommen, A. P. B.; Stoop, F.; van der Wiele, K. *Appl. Catal.* **1985**, *14*, 277−288.

(33) Koeken, A. C. J.; Torres Galvis, H. M.; Davidian, T.; Ruitenbeek, M.; de Jong, K. P. *Angew. Chem., Int. Ed.* **2012**, *51*, 7190−7193.

(34) Shroff, M. D.; Kalakkad, D. S.; Coulter, K. E.; Köhler, S. D.; Harrington, M. S.; Jackson, N. B.; Sault, A. G.; Datye, A. K. *J. Catal.* **1995**, *156*, 185−207.

(35) Soled, S.; Iglesia, E.; Fiato, A.. *Catal. Lett.* **1990**, *7*, 271−280.